Asociación Argentina
de Mecánica Computacional

Mecánica Computacional Vol XLII, pp. 413-422
A. Caggiano, G. Etse, P. Folino, M. Goldschmit, M. Pucheta, M. Storti (Eds.)
L. Battaglia, H. Castro, M. Coussirat, R. Paz, S. Sarraf, A. Scarabino (Issue eds.)
Buenos Aires, November 11-14, 2025

EVALUATION OF NUMERICAL SIMULATION STRATEGIES APPLIED TO HYDRAULIC TURBOMACHINERY

Tomás Leschiutta[a,c], Miguel G. Coussirat[b], Flavio Moll[b] and Santiago Márquez Damián[a,c]

[a]*Centro de Investigación de Métodos Computacionales (CIMEC),CONICET/UNL, Predio CONICET Santa Fe - Colectora Ruta Nac Nro 168, Paraje El Pozo, Santa Fe, Argentina, cimec@cimec.unl.edu.ar, http://www.cimec.conicet.gov.ar*

[b]*Laboratorio de Modelado Aeroplasticidad, LaMA, Universidad Tecnológica Nacional, FRM, Coronel Rodríguez 273, Mendoza, Argentina, http://www.frm.utn.edu.ar*

[c]*Universidad Tecnológica Nacional, FRSF, Lavaise 610, Santa Fe, Argentina, http://www.frsf.utn.edu.ar/*

Keywords: Hydraulic turbomachinery, Centrifugal pump, Fluid–structure interaction, CFD, OpenFOAM®.

Abstract. The design of hydraulic turbomachines operating at the so-called design point has advanced to a stage where further improvements can only be achieved through a detailed understanding of the internal flow behavior. As an alternative to physical experimentation, numerical methods have become a powerful tool for predicting internal flow characteristics. However, these predictions involve several complex challenges, including the rotating reference frame, the three-dimensional geometry of the impeller, the unsteady and turbulent nature of the flow, and fluid–structure interactions, especially under off-design conditions, where strong interactions between the impeller and the stator or casing occur. These simulations are often computationally demanding due to the fine mesh resolution required and the inclusion of various sub-models, such as moving reference frames, turbulence modeling, and, in some cases, cavitation models when operating away from the design point. This work focuses on evaluating the interplay among different modeling strategies, particularly sub-models related to rotating frames and turbulence. Various combinations of these models are tested to achieve accurate predictions of the mean flow behavior in a radial pump, accounting for some of their important geometrical characteristics. Both open-source and commercial CFD solvers are employed. The simulation results are compared against a standard experimental dataset defined for benchmarking studies.

ISSN: 2591-3522 DOI: 10.70567/mc.v42.ocsid8303

1 INTRODUCTION

Hydraulic turbomachinery has been employed since ancient times. A general classification of them is: power-producing turbomachines and power-absorbing turbomachines. Within the latter classification, pumps, fans, and blowers are a designed with the purpose of increasing the pressure of a fluid (Dixon and Hall, 2013). Although evidence exists of more rudimentary devices, the first true centrifugal pumps did not appear until the late 1600's, when Denis Papin built a prototype with straight blades (Reti, 1963). This design was later surpassed by the British inventor John Appold in 1851, who pioneered the mass production of pumps with curved blades. Subsequently, due to the growing demand for engines in vehicle and aircraft propulsion, centrifugal pumps underwent significant development. Since they could be designed more compactly than other kinds of pumps for the same efficiency, they became the preferred choice as the main component in engines.

Pumps are designed for specific operating conditions defined by the volumetric flow rate and the energy imparted to the fluid, the latter being expressed in terms of the pressure difference between inlet and outlet (also referred to as manometric head, H_m). This has led to the construction of pump series with geometric similarity in order to meet varying requirements of flow rate and energy demand, while ensuring efficient machine performance. In general, centrifugal machines exhibit a relatively narrow region of approximately 15% around the optimal design flow rate where efficiency is maximized (Coussirat et al., 2014). Outside this range, performance tends to drop off sharply.

The flow inside a pump, as in any hydraulic turbomachine, is characterized by being turbulent and passing through cavities that vary with time. Historically, the design and performance assessment of these machines has therefore relied more on experimentation than on theory, since the classical mathematical models that describe them are complete but difficult to solve because of the complexity of the machine geometry. Today, the demand for very smooth performance curves with broad regions of high efficiency and low vibration levels makes their careful design essential. This unsteady and turbulent nature of the flow gives rise to cyclic rotor–stator interaction (RSI) phenomena, which are not always clearly understood and can lead to premature machine failure

According to Dring et al. (1982) and Arndt et al. (1989), RSI can be divided into two distinct mechanisms. On the one hand, potential interaction, caused by geometric variations of the machine during the unsteady process. On the other hand, wake interaction, which consists of interferences produced by the turbulent flow between the impeller and the guide vanes, also generating pressure fluctuations.

Due to the increasingly sophisticated nature of these equipment designs, experiments have become very costly, and current trends in fluid-dynamic design involve the extensive use of computational methods for their study and development. Within this framework, computational fluid dynamics (CFD) has become one of the most widely employed techniques, enabling the prediction of complex behaviors and phenomena that are sometimes even unattainable by traditional experimental methods. Some of the geometrical characteristics play a paramount role in the RSI characterization, e.g., the flow into the machine is strongly affected by the clearance between blades and casing (Petit and Nilsson, 2013), the centrifugal pump casing section area, the interference of the impeller, the volute tongue length, and the volute tongue angle (Chia-Nan et al., 2022) or the match of rotor and stator blades leading to significant variations in the velocity maps near the tongue region (Zhou et al., 2025). It is not easy to account for these geometrical details and scarce information is in the open literature. Therefore, the ob-

jective of this work is to investigate different simulation strategies, including conformal and non-conformal meshes, together with a comparison between commercial software (Ansys Fluent, AF) and open-source software (OpenFOAM®, OP), taking into account fine geometrical details. The results will be validated against the experimental data reported by Ubaldi et al. (1998). The authors have an extensive track record in the study of RSI, and their experimental investigations have been adopted as a reference case for joint research by a working group of the Société Hydrotechnique de France and the Turbomachinery Group of the European Research Community on Flow, Turbulence and Combustion (ERCOFTAC).

A simpler case is proposed: the flow in the impeller under axisymmetric flow conditions imposed by a vaneless diffuser. This configuration is of particular interest and appropriate as a starting point for numerical predictions and comparative studies. Two-dimensional and three-dimensional simulations of the pump will be performed. The Moving Reference Frame (MRF) approach will be employed for cases with non-split meshes, while Sliding Mesh Model (SMM) or Arbitrary Mesh Interface (AMI) will be used for domains with effective relative motion. Finally, the model will be simplified to incorporate the clearance between the blade and the casing, analyzing the effects or errors incurred when this feature is not included in the prediction of the flow behavior.

2 METHODOLOGY

The complete methodology followed in this work is presented, highlighting that it can be applied to any class of hydraulic turbomachinery. First, the differences in the Navier-Stokes equations when they are expressed in steady and moving reference frames are briefly discussed. Then, the different modeling strategies in moving reference frames are presented. Finally, a detailed description of the studied cases is given.

2.1 Navier–Stokes Equations

In this work, a turbulent, incompressible and unsteady flow will be considered. For this case, the Navier–Stokes equations are:

$$\begin{cases} \dfrac{\partial}{\partial t}(\rho\vec{u}) + \vec{\nabla}\cdot(\rho\vec{u}\otimes\vec{u}) = -\vec{\nabla}p + \vec{\nabla}\cdot\left[\mu\left(\vec{\nabla}\vec{u} + \vec{\nabla}\vec{u}^{T}\right)\right] + \rho\vec{g} \\ \vec{\nabla}\cdot\vec{u} = 0 \end{cases} \tag{1}$$

By averaging the above equation, we obtain the expression of the Reynolds-Averaged Navier Stokes (RANS) equations:

$$\frac{\partial(\rho U_i)}{\partial t} + \frac{\partial(\rho U_i U_j)}{\partial x_j} = -\frac{\partial P}{\partial x_i} + \frac{\partial}{\partial x_j}\left[\mu\left(\frac{\partial U_i}{\partial x_j} + \frac{\partial U_j}{\partial x_i}\right) - \rho\overline{u_i' u_j'}\right] \tag{2}$$

where U, u', μ and $-\rho\overline{u_i' u_j'}$ represent the mean flow velocity, the velocity fluctuations due to turbulence, and the Reynolds stress tensor term, respectively.

The Reynolds averaging process generates an additional stress term (the Reynolds tensor). To solve the RANS equations, it is necessary to express the Reynolds tensor in terms of mean flow quantities. By means of the turbulent viscosity hypothesis or Boussinesq hypothesis, the solution for this term is:

$$-\rho\overline{u_i' u_j'} = \mu_t\left(\frac{\partial U_i}{\partial x_j} + \frac{\partial U_j}{\partial x_i} + \frac{2}{3}\frac{\partial U_k}{\partial x_k}\delta_{ij}\right) - \frac{2}{3}\rho k\delta_{ij} \tag{3}$$

where μ_t and k denote the turbulent viscosity and the turbulent kinetic energy, respectively.

Equation (3) combines the tangential and normal components of the Reynolds tensor, which must be solved prior to Eq. (2). The methodology for solving Eq. (3) involves the appropriate selection of a turbulence model to compute the turbulent viscosity (μ_t).

2.2 Modeling with Conformal and Non-Conformal Meshes

In the numerical modeling of turbomachinery flows, it is necessary to represent the relative motion between the rotating and stationary components. This effect can be modeled either with or without explicit mesh motion. Following the latter approach, the Moving Reference Frame (MRF) methodology introduces rotation through a change of reference frame, assuming that the flow is steady within the rotating domain. In this way, it is possible to simulate rotating components using a single conformal mesh, which significantly reduces computational cost and allows capturing the mean effects of rotation and RSI. However, the transient features of the flow and unsteady interactions cannot be fully represented, since the method relies on a quasi–steady assumption. The formulation of this method fundamentally modifies the momentum equation. The Navier–Stokes equation for the rotating region becomes:

$$\begin{cases} \dfrac{\partial \vec{u_R}}{\partial t} + \dfrac{\partial \vec{\Omega}}{\partial t} \times \vec{r} + \vec{\nabla} \cdot (\vec{u_R} \otimes \vec{u_I}) + \vec{\Omega} \times \vec{u_I} = -\vec{\nabla}(p/\rho) + \vec{\nabla} \cdot \left[\nu \left(\vec{\nabla} \vec{u_I} + \vec{\nabla} \vec{u_I}^T \right) \right] + \vec{g} \\ \vec{\nabla} \cdot \vec{u_I} = 0 \end{cases} \tag{4}$$

where $\vec{u_I}$ and $\vec{u_R}$ denote the inertial velocity and the rotating velocity, respectively, and $\vec{u_I}$ is equal to $\vec{u_R} + \vec{\Omega} \times \vec{r}$ (Lai et al., 2010; Hamdamov et al., 2023).

In contrast to the previous approach, this method employs techniques that generate relative motion between meshes. Through Sliding Mesh Modeling (SMM), available in Ansys Fluent, or Arbitrary Mesh Interface (AMI) combined with *dynamicMesh*, available in OpenFOAM®, it is possible to assign a rotation to the rotor mesh and ensure numerical communication with the stationary region. In this way, the transient and time-dependent flow structures generated by rotor–stator interaction (RSI) are inherently captured, including periodic fluctuations and wake transport. Although the computational cost is higher, these methodologies provide greater accuracy in reproducing the instantaneous flow field.

2.3 Description of Case Studies

Prior to undertaking more complex studies involving RSI analysis (Ubaldi et al., 1996), it is proposed to validate the experiment carried out by Ubaldi et al. (1998). The centrifugal pump consists of an unshrouded impeller with a diameter of 420 mm, equipped with seven single-curvature blades inclined backward, followed by a vaneless diffuser with parallel endwalls. Air enters and leaves the pump under atmospheric conditions. The blade span (b) is 40 mm. There is a clearance between the impeller blades and the casing set to 0.4 mm, which results in an effective channel height between blades of 40.4 mm. The experiment was carried out at a constant rotational speed of 2000 rpm, at the nominal operating point: flow rate coefficient $\phi = Q/(U_2 \pi R_2^2) = 0.048$, total pressure rise coefficient $\psi = 2(p_{t_{Outlet}} - p_{t_{Inlet}})/(\rho U_2^2) = 0.58$.

Based on experimental dataset, a first set of simulations were carried out, see Figure 1, considering the stator without blades and comparing results obtained without and with clearance. It features an inlet face of 184 mm in diameter, positioned 200 mm upstream of the pump base, where a volumetric flow rate of 0.292 m^3/s is imposed. The figure also specifies the cutting

section that separates the impeller and diffuser volumes, in the simulation cases where relative motion between non-conformal meshes is required. The relevant geometrical data of the model and the operating conditions are summarized in Table 1.

Component	Parameter	Value
Impeller	Inlet blade diameter, D_1	240 mm
	Outlet diameter, D_2	420 mm
	Blade span, b	40 mm
	Number of blades, z	7
Diffuser	Outlet diameter, D_4	750 mm
	Axial width, b_d	40.4 mm
Operating conditions	Flow rate, Q	0.292 m^3/s
	Rotational speed, n	2000 rpm
	Angular speed, Ω	209.44 rad/s
Inlet air conditions	Temperature, T	298 K
	Density, ρ	1.2 kg/m^3
	Kinematic viscosity, ν	1×10^{-5} m^2/s

Table 1: Geometrical and operating parameters of the centrifugal pump.

Before proceeding with the 3D simulations, and as an initial validation step, 2D model cases of the experiment were generated. The main difference was that the inlet was simplified to a cylindrical area with a 200 mm diameter, following the approach of Petit et al. (2009). Finally, all the simulated cases are summarized in Table 2.

Model	Software	Method	Case	Comments
2D	OpenFOAM	MRF	1	207,318 cells
		AMI	2	207,718 cells
	Ansys Fluent	MRF	3	365,000 cells
		SMM	4	365,000 cells
3D	Ansys Fluent	MRF	5	1,451,000 cells
		MRF	6	1,137,000 cells one channel, with clearance

Table 2: Summary of numerical simulation cases.

It should be noted that Case 6 is three–dimensional but makes use of Ansys Fluent's capability to simulate only a single channel of the pump. In addition, in this last case the clearance between the blades and the casing was modeled. To this end, a mesh was incorporated in that region and a periodic boundary condition was applied between blades in order to capture the flow through the clearance and the associated head loss.

Regarding the numerical modeling, all cases were computed using the k-ω SST turbulence model. A detailed summary of the turbulence models employed can be found in Coussirat et al. (2016) and Cortes and Damián (2024). The setup of these cases included a defined turbulence intensity (Tu) of 5% and a viscosity ratio (μ_t/μ) of 10 at the turbomachinery inlet. Second–order spatial and temporal schemes were used for the simulations, and the maximum Courant number was kept below 1.

For the comparison of results, circumferential sampling was performed in all cases at radio of $r/R_2 = 0.676$, 0.810, 0.952, and 0.995 (see Fig. 1).

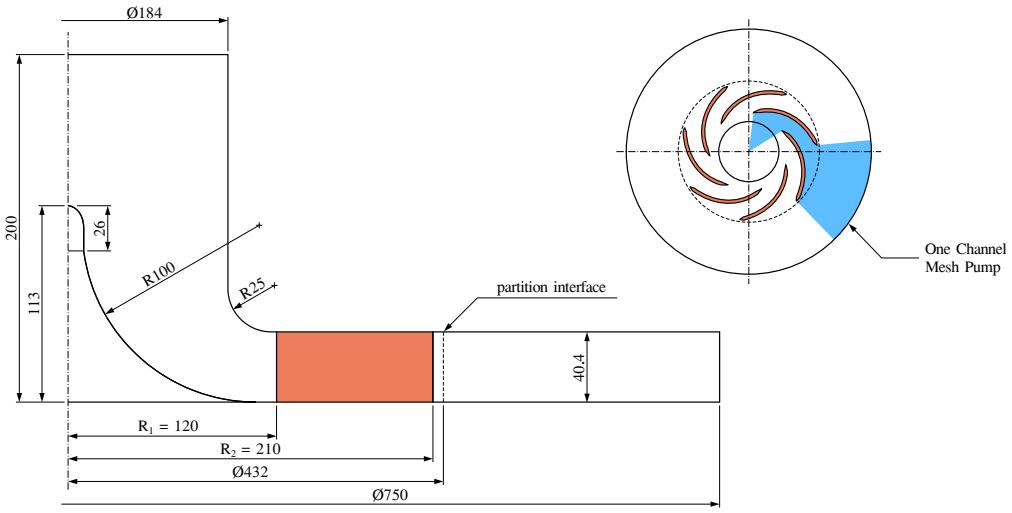

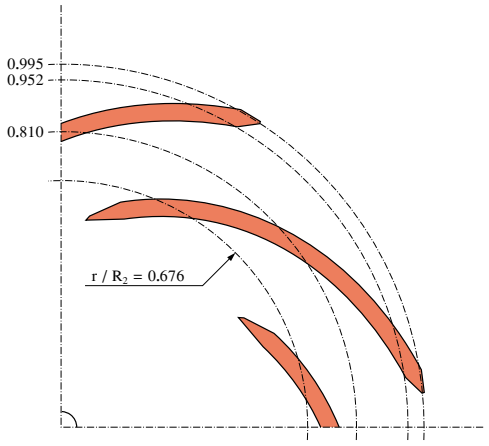

Impeller blade profile coordinates

Suction side				Pressure side			
r (mm)	θ (deg)	r (mm)	θ (deg)	r (mm)	θ (deg)	r (mm)	θ (deg)
120.00	0.00	158.22	41.01	120.00	0.00	167.52	39.72
120.48	1.61	162.49	44.79	122.76	1.16	171.81	43.54
121.06	3.21	166.77	48.52	124.91	2.79	176.11	47.33
121.74	4.79	171.05	52.22	126.76	4.10	180.40	51.06
122.50	6.36	175.33	55.87	128.71	5.40	184.69	54.75
123.36	7.91	179.61	59.47	130.77	6.69	188.98	58.39
124.31	9.43	183.89	63.02	132.95	7.96	193.27	61.97
128.31	13.62	188.17	66.52	137.43	11.86	197.56	65.49
132.58	17.67	192.45	69.95	141.73	15.98	201.85	68.95
136.86	21.65	196.74	73.31	146.03	20.04	206.13	72.34
141.13	25.60	201.02	76.61	150.33	24.05	210.42	75.66
145.40	29.50	203.83	77.59	154.63	28.03	210.34	77.00
149.67	33.37	206.67	78.52	158.92	31.96	210.36	78.23
153.94	37.21	209.53	79.42	163.22	35.86	210.47	79.33

Figure 1: Descriptive scheme of simulated models.

3 RESULTS AND DISCUSSION, CASES 2D AND 3D

Although the geometry is considered simplified, three-dimensional effects cannot be disregarded. Nevertheless, the 2D results provide a quick overall view of the flow evolution inside the impeller. Figure 2 shows the results obtained for cases 1, 2, 3, and 4, together with the reference data. The plotted values correspond to the relative velocity of the flow along the circumferential position of the sampling point within the blade-to-blade channel (see Figure 1). It should be noted that both quantities were nondimensionalized with the impeller outlet peripheral velocity, $U_2 = \Omega \times R_2 = 43.982$ m/s, and the circumferential pitch length, $G_i = 2\pi r/z$, respectively. It is remarked here that G_i takes into account the circumferential solid blade section.

Averages across the channel height were computed for their representation, see Figure 2, from its reference values, see Figure 3. All the velocity profile data from Figure 2 were initially extracted from the experimental information, i.e., a similar figure as Figure 3, provided by (Ubaldi et al., 1998) but in a gray scale. This figure was processed to obtain the color map shown in Figure 3. Owing to the experimental sampling methodology (Ubaldi et al., 1998), the regions of the channel near the blades were not fully captured, resulting in mean values within the boundary layer that are physically inaccurate; for practical purposes, these values were disregarded in the present work.

As explained by Ubaldi et al. (1998), from inlet to outlet, the streamwise evolution of the

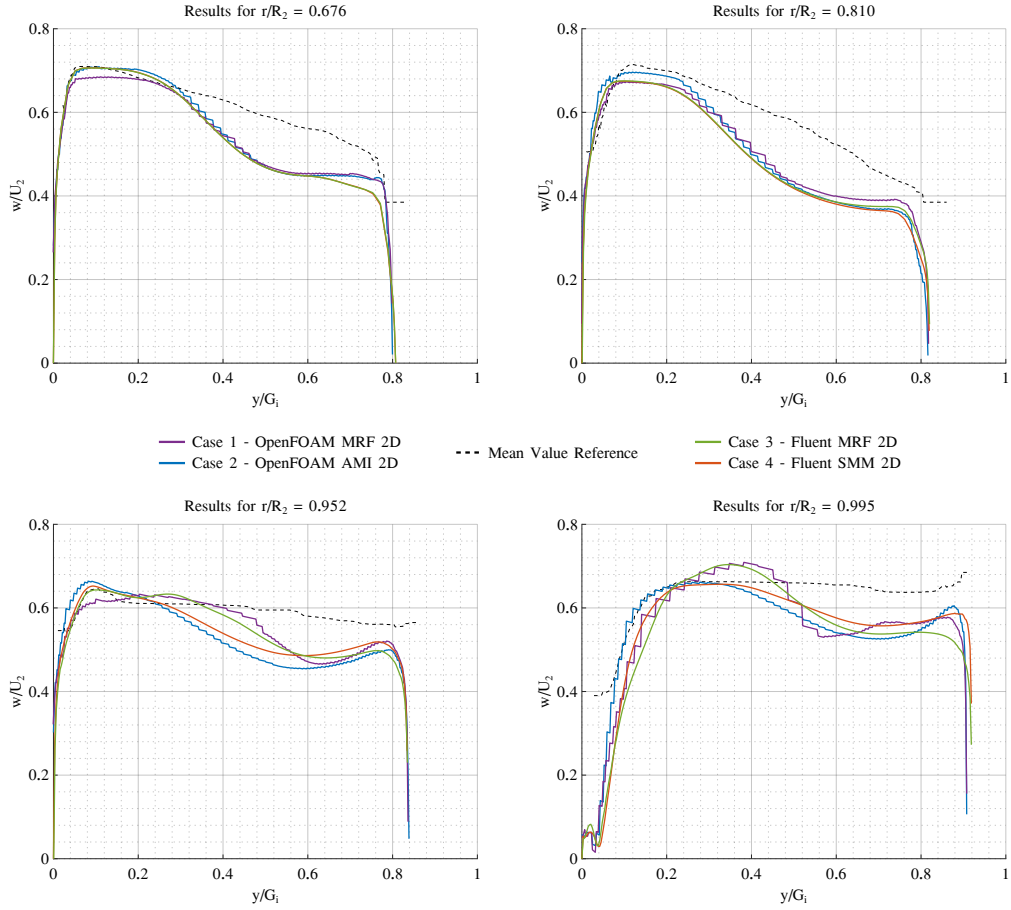

Figure 2: Comparison of relative velocities within the impeller between cases 1, 2, 3 and 4 and average experimental value over the blade height

relative velocity w indicates that, in this low-load impeller, the flow velocity does not decrease significantly since most of the pressure rise is obtained by centrifugal effects. As shown in the figure, despite their limitations, all four cases are able to capture the evolution of w across the different sampling planes. The location of the maximum aerodynamic load at $r/R_2 = 0.810$ was successfully captured, as well as its decrease as the flow progresses through the channel.

When comparing the methods, as the flow approaches the impeller outlet, both software packages overpredict w on the suction side when using the MRF approach. This error is most likely related to the proximity to the boundary of the predefined region of application for that methodology.

Three-dimensional modeling allows us to observe the vertical distribution of the flow within the channels. Figure 3 further clarifies the description given in the previous section regarding the circumferential aerodynamic loading. Its value increases initially, reaching a maximum at sampling station 2 ($r/R_2 = 0.810$), and decreases as the flow approaches the end of the channel, where it has already absorbed the energy delivered by the impeller.

At $r/R_2 = 0.810$, the nearly vertical contour lines indicate a substantially two-dimensional flow structure at this station, which is altered in the casing/pressure-side corner by the accumulation of low-momentum fluid generated by the tip leakage vortex (Ubaldi et al., 1998). This low-momentum fluid is most likely produced by two concomitant phenomena: a flow separation in the bladeless region, where a strong meridional curvature exists at the casing inlet, and

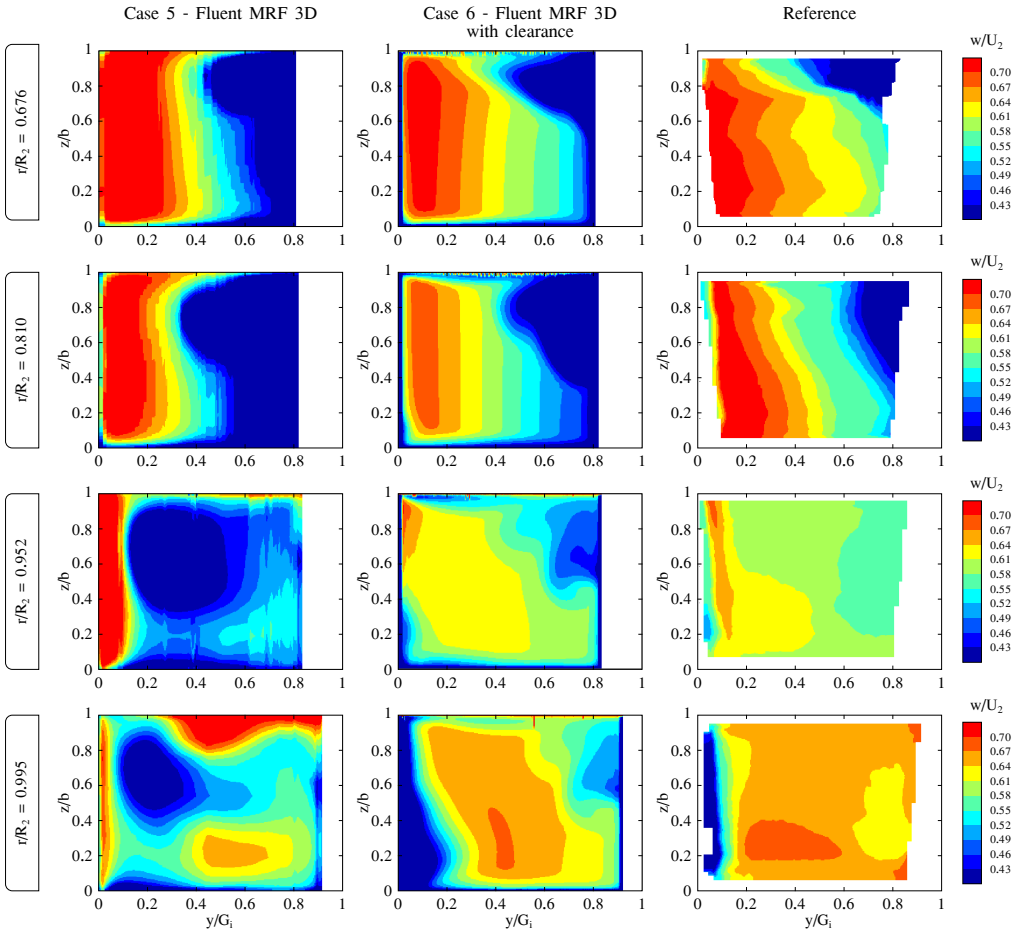

Figure 3: Comparison of relative velocities inside the impeller between 3D cases with and without clearance modeling, and corresponding reference values.

the tip leakage effect.

As shown in Figure 3, there is a direct dependence of the simulation's predictive capability on the modeling of the clearance between the blades and the casing. This associated effect becomes more pronounced in the final section of the channel, allowing the capture of the drop in aerodynamic loading and the growth of the boundary layer on the blade's suction side near the trailing edge.

Finally, as a complement to the cross–sectional flow analysis, Figure 4 shows the relative velocity field on a midspan section at blade height. In this case the influence of the inlet geometry of the pump over the flow at the vane inlet, see Fig. 1, is analyzed from other viewpoint by comparing it against experiments from Ubaldi et al. (1998). Despite that experiments do not give a complete information of the boundary layer details, comparisons of the obtained results allows to check the suitable boundary layer "mean shape" predicted along the blade. As can be observed, the grayscale map agrees very well with the experimental measurements.

This representation contributes to an overall view of the flow evolution inside the impeller. The relative velocity along the midspan line does not decrease significantly from the impeller inlet to its outlet, and only a low–velocity region can be identified on the pressure side. Because the machine operates under design conditions, the boundary layers on both blade surfaces remain attached throughout the entire channel. From another perspective, the growth of the boundary layer on the suction side toward the impeller exit can also be clearly confirmed.

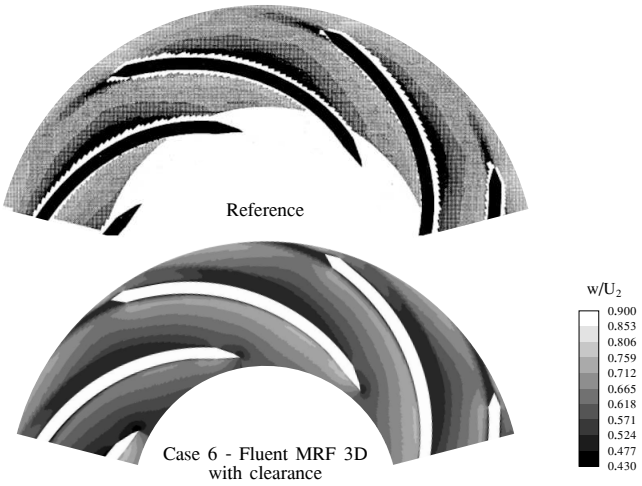

Figure 4: Relative velocity comparison between Case 6 and the reference in the blade-to-blade plane.

4 CONCLUSIONS

In this work, numerical studies were carried out on the experimental case reported by Ubaldi et al. (1998). The setup consists of a centrifugal pump with a seven backward–curved blades impeller, followed by a vaneless diffuser. The impeller is unshrouded because a 0.4mm gap between the casing and the blade tip is present. Different simulation strategies were employed, including both conformal and non-conformal meshes, and the Moving Reference Frame, Sliding Mesh Modeling, and Arbitrary Mesh Interface approaches as modeling methodologies. In addition, the simulations incorporated the modeling of the clearance between the rotating blades and the stationary casing, an aspect not widely described in the literature.

Both the 2D and 3D results successfully captured the flow development inside the channels and the boundary layer development along the blades. The increase in aerodynamic load up to the sampling station 2 ($r/R_2 = 0.810$) and its subsequent decrease near the channel outlet were correctly reproduced.

A comparison of the applied methodologies for different mesh configurations was made. Using MRF with conformal meshes provides results at a lower computational cost, albeit with somewhat reduced accuracy. Far from being a drawback, this feature is valuable as a tool for generating initial flow fields for more complex and computationally expensive simulations involving actual mesh motion.

The results obtained also indicate that explicitly modeling the clearance between blades and casing is unavoidable in order to achieve accurate predictions of the experimental test. Nevertheless, it remains necessary to carry out further analyses with different mesh resolutions to rule out any significant sensitivity of the results to grid discretization.

As future work, a comparative analysis of computational cost between the different software platforms and simulation methodologies will be undertaken.

ACKNOWLEDGEMENTS

The authors acknowledge the financial support provided by CONICET (doctoral fellowship of Tomás Leschiutta) and UTN FRM. This work is a part of the project PID-UTN-8685, “Numerical methods for low Reynolds number flows with applications in civil and mechanical engineering.” and the project SCTyP: AMTCAME0008441TC, from UTN FRM.

REFERENCES

Arndt N., Acosta A.J., Brennen C.E., and Caughey T.K. Rotor–Stator Interaction in a Diffuser Pump. *Journal of Turbomachinery*, 1989. http://doi.org/10.1115/1.3262258.

Chia-Nan W., Fu-Chiang Y., Van Thanh Tien N., and Nhut T.V. CFD Analysis and Optimum Design for a Centrifugal Pump Using an Effectively Artificial Intelligent Algorithm. *Micromachines*, 2022.

Cortes F.L. and Damián S.M. Modificación del Modelo k-omega SST para la Obtención del Perfil de Energía Cinética Turbulenta: Flujo en Placa Plana. *Mecánica Computacional*, 41, 2024.

Coussirat M.G., Fontanals García A., Panella L., and Guardo Zabaleta A.d.J. Estudio del Fenómeno de Interacción Rotor Estator (RSI) en una Bomba Radial, Trabajando Fuera de las Condiciones de Diseño Óptimo. *Asociación Argentina de Mecánica Computacional*, 2014.

Coussirat M.G., Moll F.H., and Fontanals A. Capability of the Present Cavitating and Turbulence Models for Confined Flow Simulations. *Mecánica Computacional*, 34, 2016.

Dixon S.L. and Hall C. *Fluid Mechanics and Thermodynamics of Turbomachinery*. Butterworth-Heinemann, 2013.

Dring R.P., Joslyn H.D., Hardin L.W., and Wagner J.H. Turbine Rotor-Stator Interaction. *Journal of Engineering for Power*, 104(4):729–742, 1982. http://doi.org/10.1115/1.3227339.

Hamdamov M., Bozorov B., Mamataliyeva H., and Ergashov D. Numerical Modeling of Wind Turbine with Vertical Axis using Turbulence Model k- ω in Ansys Fluent. In *E3S Web of Conferences*, volume 401, page 02024. EDP Sciences, 2023.

Lai W.M., Rubin D., and Krempl E. *Introduction to Continuum Mechanics (Fourth Edition)*, chapter 7. Butterworth-Heinemann, 2010.

Petit O. and Nilsson H. Numerical Investigations of Unsteady Flow in a Centrifugal Pump with a Vaned Diffuser. *International Journal of Rotating Machinery*, 2013(1):961580, 2013.

Petit O., Page M., Beaudoin M., and Nilsson H. The ERCOFTAC Centrifugal Pump OpenFOAM Case-Study. In *Proceedings of the 3rd IAHR International Meeting of the Workgroup on Cavitation and Dynamic Problem in Hydraulic Machinery and Systems, Brno, Czech Republic*, pages 14–16. 2009.

Reti L. Francesco di Giorgio Martini's Treatise on Engineering and its Plagiarists. *Technology and Culture*, 4(3):287–298, 1963.

Ubaldi M., Zunino P., Barigozzi G., and Cattanei A. An Experimental Investigation of Stator Induced Unsteadiness on Centrifugal Impeller Outflow. *Journal of Turbomachinery*, 118, 1996. http://doi.org/10.1115/1.2836604.

Ubaldi M., Zunino P., and Ghiglione A. Detailed Flow Measurements within the Impeller and the Vaneless Diffuser of a Centrifugal Turbomachine. *Experimental Thermal and Fluid Science*, 17, 1998.

Zhou D., Zhang N., Zheng F., Gad M., and Gao B.G. Experimental Investigation on the Effect of the Rotor-Stator Matching Mode on Velocity Pulsation in the Centrifugal Pump with a Vaned Diffuser. *Nuclear Engineering and Technology*, 57(3):103255, 2025.